DNN Pruning and Its Effects on Robustness

Sven Mantowksy, Firas Mualla, Saqib Sayad Bukhari and Georg Schneider
ZF Friedrichshafen AG, AI-Lab, Saarbrücken, Germany

Keywords: Pruning, Explainability, Calibration.

Abstract: The popularity of deep neural networks (DNNs) and their application on embedded systems and edge devices is increasing rapidly. Most embedded systems are limited in their computational capabilities and memory space. To meet these restrictions, the DNNs need to be compressed while keeping their accuracy, for instance, by pruning the least important neurons or filters. However, the pruning may introduce other effects on the model, such as influencing the robustness of its predictions. To analyze the impact of pruning on the model robustness, we employ two metrics: heatmap based correlation coefficient (HCC) and expected calibration error (ECE). Using the HCC, on one hand it is possible to gain insight to which extent a model and its compressed version tend to use the same input features. On the other hand, using the difference in the ECE between a model and its compressed version, we can analyze the side effect of pruning on the model's decision reliability. The experiments were conducted for image classification and object detection problems. For both types of issues, our results show that some off-the-shelf pruning methods considerably improve the model calibration without being specifically designed for this purpose. For instance, the ECE of a VGG16 classifier is improved by 35% after being compressed by 50% using the H-Rank pruning method with a negligible loss in accuracy. Larger compression ratios reduce the accuracy as expected but may improve the calibration drastically (*e.g.* ECE is reduced by 77% under a compression ratio of 70%). Moreover, the HCC measures feature saliency under model compression and tends to correlate as expected positively with the model's accuracy. The proposed metrics can be employed for comparing pruning methods from another perspective than the commonly considered trade-off between the accuracy and compression ratio.

1 INTRODUCTION

The popularity of deep neural networks (DNNs), especially convolutional neural networks, has increased over the last few years. Their applications have become indispensable in areas such as computer vision, robotics (Brunke et al., 2022), natural language processing (Otter et al., 2020) and optimization of industrial processes (Weichert et al., 2019). For a while now, neural networks can even outperform humans in different tasks such as voice and object recognition, which emphasizes their usability even more. However, to achieve such an outstanding performance, neural networks are becoming more complex, leading to over-parameterization and more computationally expensive operations. This situation necessitates large computational capacity, more memory and an overall increase in power consumption. These complexities impede the transition of a deep learning model into a product-level application, especially when embedded systems or edge devices are used. In particular, the automotive field has strict requirements regarding computationally expensive algorithms such as deep learning models. For this reason, researchers are investigating various pruning methods to reduce the size of neural networks. The most common approach is to identify and to remove the least important network components, while avoiding any adverse effect on overall accuracy. This sort of model's compression enables the deployment of large deep learning models on resource-constrained edge devices. Most pruning algorithms focus only on simple key performance indicators (KPI), such as accuracy and inference time after pruning. However, these KPIs cannot provide a deeper insight into other changes introduced by pruning, such as regarding model robustness.

To resolve this problem, we present two metrics to analyze the robustness of compressed models. The first metric uses the correlation between a pair of heatmaps, generated for an input sample for the model and its pruned version. With the help of these heatmaps, we can evaluate which features are decisive for a prediction. Comparing two different heatmaps of an unpruned and pruned model can show if the areas of interest change after pruning. It is called Heatmap Correlation Coefficient (HCC). The

Mantowksy, S., Mualla, F., Bukhari, S. and Schneider, G.
DNN Pruning and Its Effects on Robustness.
DOI: 10.5220/0011651000003411
In *Proceedings of the 12th International Conference on Pattern Recognition Applications and Methods (ICPRAM 2023)*, pages 82-88
ISBN: 978-989-758-626-2; ISSN: 2184-4313

heatmaps are generated using Deep Taylor Decomposition (DTD) method (Montavon et al., 2017b). Since the original version of DTD is limited to image classification problem, we use a further developed in-house version of the DTD method for object detection. The second metric employs miscalibration measurement, particularly Expected Calibration Error (ECE) (Guo et al., 2017). In order to compare the calibration of a pruned model with its unpruned baseline we use reliability diagrams to measure the changes in the relationship between accuracy and output's confidence. We summarize our contributions as follows:

- We employ heatmaps to measure feature saliency under pruning using HCC.
- We show through experiments with ECE and reliability diagrams that pruned models can be considerably better in calibration as compared to unpruned models, even without using a pruning method specifically designed for this purpose.
- The proposed metrics are flexibly applicable to off-the-shelf pruning techniques and models, allowing very versatile applicability.

2 RELATED WORK

There have been frequent reports in literature emphasizing the role of pruning in improving the generalizability of neural networks to unseen examples (LeCun et al., 1989; Hassibi and Stork, 1992; Hoefler et al., 2021; Nadizar et al., 2021).

Recently, researchers (Jordão and Pedrini, 2021; Guo et al., 2018) showed that pruning tends also to improve the adversarial robustness of the resulting models even without adversarial training. The pruned models therefore tend not to inherit the adversarial vulnerability of the original models. Some other approaches combine both adversarial training and pruning to maximize robustness (Ye et al., 2019; Sehwag et al., 2020; Gui et al., 2019). This line of work has also been extended to the so-called *certifiably robust* approaches against adversarial attacks (Li et al., 2022). For these types of methods, usually, either the pruning procedure or the training is modified to improve adversarial robustness.

The works mentioned above studied the positive side effects of pruning on the robustness defined in terms of generalizability to unseen examples or immunity to adversarial attacks. In this work, however, we are interested in robustness in terms of model calibration and model-side feature saliency for off-the-shelf pruning methods.

3 METHODS

3.1 Neural Network Pruning

Pruning methods reduce the size of an already trained model to correspondingly decrease the runtime, memory footprint, and power consumption. For this purpose, redundant parameters are removed from the model while trying to preserve the model accuracy compared to the baseline model. Since pruning has a regularization effect (Bartoldson et al., 2020), it is sometimes even possible to gain some improvement in accuracy by pruning, especially when the initial network is over-parameterized.

In general, pruning methods can be divided into two main categories: structured and unstructured pruning. In structured pruning, complete structures such as layers (Wang et al., 2017), filters (Zeng and Urtasun, 2019) or channels (He et al., 2017) are removed. On the other hand, in unstructured pruning (Lee et al., 2018; Kwon et al., 2020), individual weights are set to zero (Han et al., 2015; Hayou et al., 2021). Unstructured pruning methods suffer significant drawbacks, such as particular frameworks and chip architectures are required, as not all algorithms and hardware architectures can exploit weight sparsity to improve performance. Therefore, in this work we consider only structured pruning methods for our experiments.

3.2 Heatmap Generation Using Deep Taylor Decomposition

While being known to perform very well at least for in-distribution data, deep neural networks tend to show a kind of black-box behavior compared to other more transparent machine learning paradigms such as simple linear classifiers or decision trees. Explainable Artificial Intelligence (XAI) (Arrieta et al., 2020) is a relatively new field that addresses this black-box-behavior issue. Deep Taylor Decomposition (DTD) (Montavon et al., 2017a) is an XAI method inspired by decomposing a function value (e.g. object score or class probability) as a sum of input feature contributions based on the Taylor series. The relevance R of a neuron inside a layer l of a neural network is decomposed in terms of the activations $\mathbf{a}$ of the previous layer $l-1$. More specifically, a root $\mathbf{a}_0$ of the relevance R in the space of the activations of the previous layer must be first found. A linear approximation of Taylor expansion of R can be then computed as the inner product of $(\mathbf{a}-\mathbf{a}_0)$ and the gradient of R at $\mathbf{a}_0$. This inner product is a sum of terms, each of them contributes to calculating the relevance of a neuron in

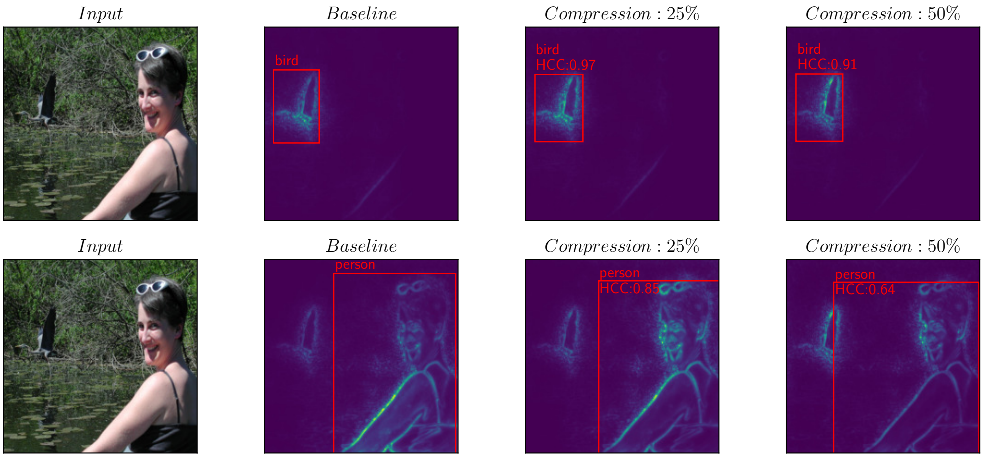

Figure 1: DTD Heatmaps are generated for each object in the image (one object per figure's row). Columns show from left to right: input image of the object detector SSD, heatmap of the unpruned model, heatmap of the model pruned by 25%, and heatmap of the model pruned by 50%. The HCC (see text) measures the feature saliency under model compression.

the previous layer $l-1$ based on the relevance of the considered neuron in layer l. The method is closely related to another XAI method called Layerwise Relevance Propagation (LRP) (Bach et al., 2015). The LRP is a scheme of different propagation rules for the redistribution of a neuron's relevance on the neurons of its previous layer. In particular, the so-called LRP γ-rule can be given as follows:

$$R_i = \sum_j \frac{z_{ij} + \gamma z_{ij}^+}{\varepsilon + \sum_k z_{kj} + \gamma z_{kj}^+} R_j, \quad (1)$$

$$z_{ij} = a_i w_{ij} \quad (2)$$

$$z_{ij}^+ = max(0, z_{ij}) \quad (3)$$

where R_j denotes the relevance of a neuron j, w_{ij} the weight connecting neuron i with neuron j, a_i the activation of the neuron i, ε is an arbitrary small number, and γ is a parameter of the rule.

Under the assumption of a relu activation function, the DTD is equivalent to the LRP γ-rule when $\gamma \to \infty$ (Samek et al., 2021). This equivalence was employed to simplify the implementation of the DTD. Both the DTD and LRP are originally designed for image classification problems. For this work, we used an extension of DTD that can be applied to both classification and object detection problems (KIA Project Booklet, 2022).

3.3 Heatmap Correlation Coefficient

We employ the heatmap concept to assess feature saliency under pruning. The correlation coefficient between the heatmap of the baseline model H^b and the heatmap of the pruned model H^p is computed as follows:

$$HCC(H^b, H^p) = \frac{\frac{1}{n}\sum_{i,j}(H^b(i,j) - \mu_{H^b})(H^p(i,j) - \mu_{H^p})}{\sigma_{H^b}\sigma_{H^p}}, \quad (4)$$

where n is the number of pixels, $\mu_{H^b}, \sigma_{H^b}, \mu_{H^p}, \sigma_{H^p}$ are the mean and standard deviation of the baseline and the pruned models, respectively. Figure 1 demonstrates the calculation of HCC using DTD heatmaps applied to object detection.

3.4 Expected Calibration Error (ECE)

To evaluate the performance of a deep learning model, accuracy is often insufficient, as the confidence of a model's decision and not only the decision itself has to be evaluated. Reliability diagrams are usually employed to measure the deviation between the model's confidence and measured accuracy. The identity function would represent a perfect calibration (shown as a dashed line in the ECE figures below). Any deviation from this identity function means a miscalibration of the model, and the model is considered accordingly either overconfident or underconfident. The confidence in this scenario is represented by the models probability outputs. Inside each small interval (bin) B_m of the confidence, the deviation between measured accuracy $acc(B_m)$ inside this bin and the center of the bin $conf(B_m)$ can be calculated. The expected calibration error is defined as the expectation (weighted sum) of these deviations:

$$ECE = \sum_{m=1}^{M} \frac{|B_m|}{S} \left| acc(B_m) - conf(B_m) \right|, \quad (5)$$

where $|B_m|$ is the number of samples inside the bin, M is the number of bins, and S is the number of samples.

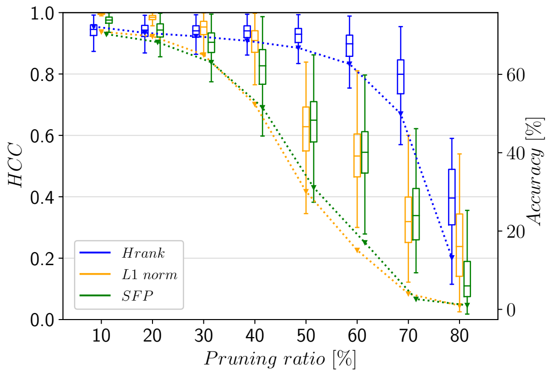

Figure 2: Boxplot of HCC of heatmap pairs for the VGG16, compressed with different pruning methods and compression ratios. The dotted lines show the accuracy of each pruned model at the corresponding pruning ratio. The boxplots are grouped to a compression rate of 10%.

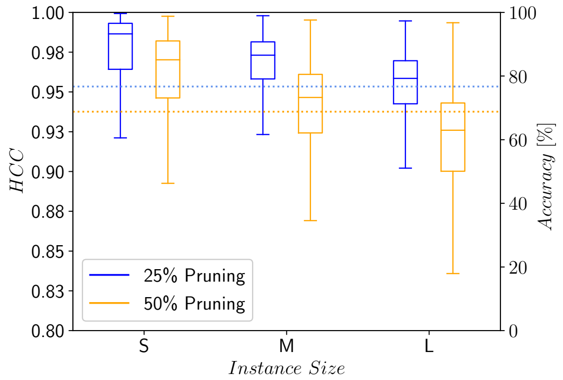

Figure 3: Distribution of HCC for the SSD, compressed with the HRank method with two different compression rates, categorized by object sizes. The dotted line shows the accuracy of each model. The PASCAL VOC dataset was used for both experiments.

In some contexts, especially in safety-critical applications, the maximum deviation between confidence and accuracy can be additionally considered:

$$MCE = \max_{m \in \{1,\ldots,M\}} |acc(B_m) - conf(B_m)|. \quad (6)$$

4 RESULTS

In this Section, we present the results of heatmap correlation and the impact of pruning on network calibration. We distinguish between classification using the VGG16 model (Simonyan and Zisserman, 2014) and object detection using the Single Shot Detector (SSD) (Liu et al., 2016). For classification, we used three different pruning methods: L1-norm (Li et al., 2016), HRank (Lin et al., 2020) and Soft Filter Pruning (SFP) (He et al., 2019). For object detection, we extended the HRank method to be applicable to all layers of the SSD.

4.1 Heatmap Correlation

In Section 3.3, we introduced the heatmap correlation coefficient (HCC) as a metric to analyze the impact of pruning using the heatmap methods. First, we present the results of the classification model VGG16, pruned with three different pruning methods and compression rates between 0% and 80%. Higher compression rates are negligible as the accuracy already drops to less than 5% for a compression rate of 80%. The results are visualized as a boxplot in Figure 2. The trend of HCC over different compression ratios seems to be very similar for all pruning methods. However, on closer inspection, it becomes apparent for L1-norm and SFP, that the HCC decreases continuously as the compression rate increases, which corresponds to expectations. The HCC of the HRank method, however, remains almost constant up to a compression rate of 55%, which indicates a more robust network and therefore a more robust pruning method.

As mentioned above, we adapted the HRank method to work with all layers of the SSD. After training the SSD on the PASCAL VOC dataset, we made sure that the extended HRank pruning was working fine. We were able to compress the model by up to 50%. We generated heatmap pairs under the same procedure described above, with the addition that we categorized the resulting bounding boxes according to object size. This is based on the categorization of the PASCAL VOC dataset, in which the difficulty of an object depends, among other criteria, on its size. The distribution of all HCC results for compression ratios of 25% and 50% are shown in Figure 3. A decrease in the HCC can be clearly seen as the compression rate increases and this reflects the behavior of the classification results shown previously. The difference in HCC between the 25% and 50% compressed model can also be seen more clearly for large objects. In case of large instances, it is more common for structures in the background to contribute slightly to the result. After pruning, the probabilities of contributing background pixels can increase which leads to a decrease in HCC. Figure 1 (2^{nd} row) shows such an example, in which the probabilities of the background structures increase with the compression ratio.

4.2 Network Calibration

The calibration error is an additional tool to evaluate the change in robustness after pruning compared to its baseline. The ECE is a suitable metric for this pur-

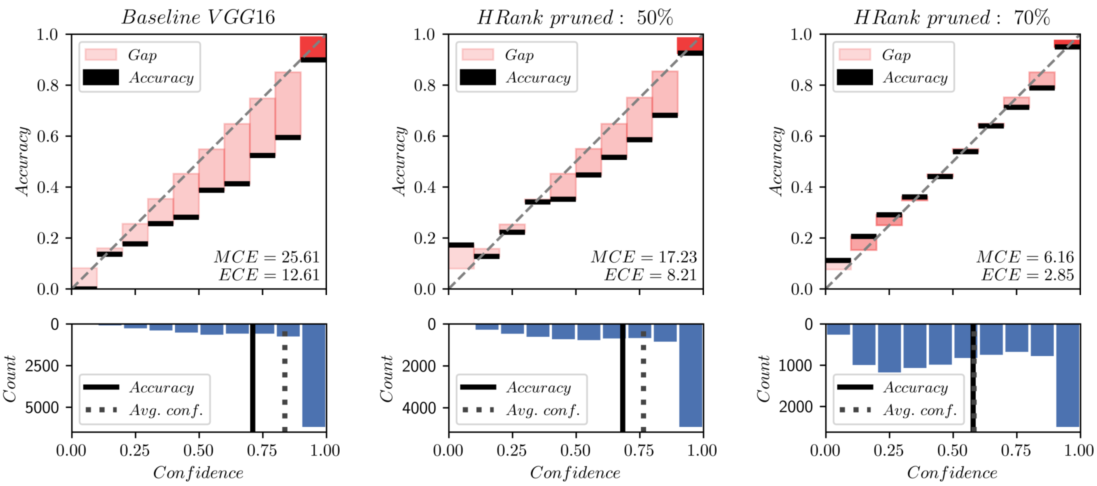

Figure 5: Reliability diagrams of VGG16: (a) unpruned model, (b) pruned with HRank method and a compression ratio of 50%, (c) pruned with HRank method and a compression ratio of 70%. The dotted line in the upper graph represents the perfect calibration. The lower graph represents the number of objects within an interval (bin).

pose, as described in Section 3.4. First, we present the results of the VGG16 model pruned with HRank, L1-norm, and SFP before proceeding to object detection. The baseline is the VGG16 trained on the CIFAR100 dataset, with an accuracy of 71.26%. While increasing the compression rate, the accuracy begins to decrease, but a significant loss for L1-norm and SFP can first be seen from 25% compression rate and for HRank from 55% compression rate onward. The ECE was calculated for each model after pruning and is shown in Figure 4. Two aspects stand out:

(i) It can be clearly seen that pruning has a positive effect on the calibration of a network. Often, at meager compression rates, accuracy even increases, giving an additional advantage through pruning. At higher compression rates, there is a trade-off between

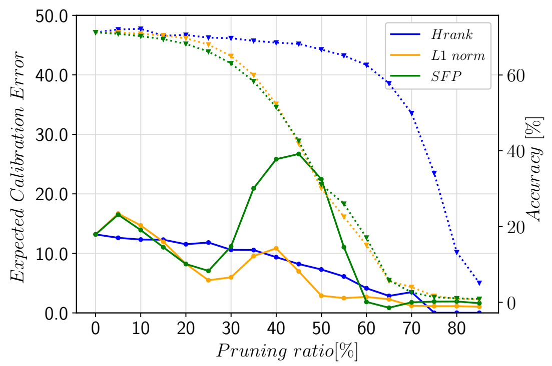

Figure 4: Comparing Expected Calibration Error for different compression ratios (0% - 85%) after pruning the VGG16 with three different pruning methods (HRank, L1 norm and SFP). The dotted line shows the accuracy of each pruned model at the corresponding pruning ratio. The sampling rate of the compression rate is 5%.

accuracy and calibration that must be considered individually.

(ii) For L1-norm and SFP, with a substantial decrease in accuracy, the ECE also increases rapidly (from 25% compression rate onwards), until the accuracy converges towards zero. In this point, the HRank method differs from the other two methods, although the reason needs to be investigated.

For a better understanding of the calibration, a reliability diagram with the values of ECE is shown in Figure 5 for a better understanding of the calibration and the value of the ECE. Compared to the baseline, the accuracy of the 50% pruned model is reduced only by 2.14%. However, the ECE has improved by 35% from 12.61 of the baseline. This is an unambiguous indication that pruning can impact and improve a network's decision and therefore making it safer and more robust. Further pruning as seen in Figure 5 (c), yields a drop in accuracy but improves model calibration. It thus improves the model's awareness of its low accuracy.

We applied the same procedure to object detection. However, due to the high expenditure of time for implementation and testing, we have limited ourselves to the HRank method. Figure 6 shows the result of an SSD pruned by a compression rate of 25%. Compared to image classification problem, there is no confidence below 0.3, as this limit is the minimum to accept a prediction final detection. As before, the result shows an improvement in ECE of nearly 10%, while the detector's accuracy decreases by less than 1%. Thus, pruning improves the calibration of object detection models as well.

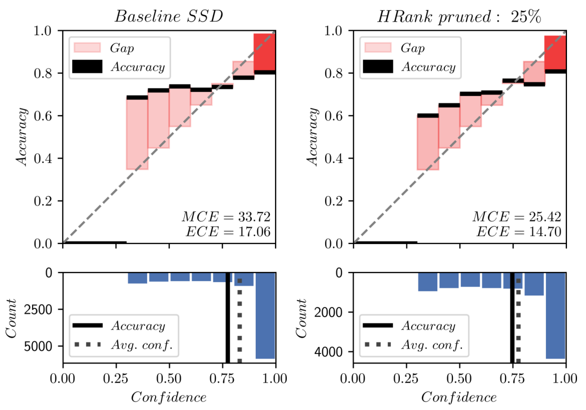

(a) (b)

Figure 6: Reliability diagram of SSD (a) unpruned and (b) pruned with HRank method and a compression ratio of 25%. The graph shows no calibration for confidences less than 0.3, since the confidence threshold for a detection is set to 0.3, based on the original publication of the SSD. The dotted line in the upper graph represents the perfect calibration. The lower graph represents the number of objects within an interval (bin).

5 CONCLUSIONS

In this paper we analyzed some side effects of off-the-shelf pruning methods on both model calibration and feature saliency. Our results show that pruning may considerably improve the model's calibration without being specifically designed for this purpose. A well-calibrated model excels at estimating the reliability of its own decisions. Pruning may thus have a positive effect on reliability and robustness. This result complements literature reports pointing out a positive contribution of the pruning to adversarial robustness.

Additionally, we employ heatmap methods from the field of XAI, particularly the similarity between the heatmap of a pruned model and the heatmap of its unpruned baseline to investigate the effects of pruning on feature saliency. As expected, pruned models tend to look at features differently than those being considered by the unpruned baseline when the accuracy drops. Therefore it makes sense in future work to enforce a kind of heatmap saliency in the model compression process to improve the accuracy of pruned models.

ACKNOWLEDGEMENTS

The research leading to these results was partially funded by the German Federal Ministry for Economic Affairs and Energy within the project "KI-Absicherung" (grant: 19A19005U).

REFERENCES

Arrieta, A. B., Díaz-Rodríguez, N., Del Ser, J., Bennetot, A., Tabik, S., Barbado, A., García, S., Gil-López, S., Molina, D., Benjamins, R., et al. (2020). Explainable artificial intelligence (xai): Concepts, taxonomies, opportunities and challenges toward responsible ai. *Information fusion*, 58:82–115.

Bach, S., Binder, A., Montavon, G., Klauschen, F., Müller, K.-R., and Samek, W. (2015). On pixel-wise explanations for non-linear classifier decisions by layer-wise relevance propagation. *PLoS ONE*, 10(7):e0130140.

Bartoldson, B. R., Morcos, A. S., Barbu, A., and Erlebacher, G. (2020). The generalization-stability tradeoff in neural network pruning.

Brunke, L., Greeff, M., Hall, A. W., Yuan, Z., Zhou, S., Panerati, J., and Schoellig, A. P. (2022). Safe learning in robotics: From learning-based control to safe reinforcement learning. *Annual Review of Control, Robotics, and Autonomous Systems*, 5:411–444.

Gui, S., Wang, H., Yang, H., Yu, C., Wang, Z., and Liu, J. (2019). Model compression with adversarial robustness: A unified optimization framework. *Advances in Neural Information Processing Systems*, 32.

Guo, C., Pleiss, G., Sun, Y., and Weinberger, K. Q. (2017). On calibration of modern neural networks. In *International conference on machine learning*, pages 1321–1330. PMLR.

Guo, Y., Zhang, C., Zhang, C., and Chen, Y. (2018). Sparse dnns with improved adversarial robustness. *Advances in neural information processing systems*, 31.

Han, S., Pool, J., Tran, J., and Dally, W. J. (2015). Learning both weights and connections for efficient neural networks. In *Proceedings of the 28th International Conference on Neural Information Processing Systems - Volume 1*, NIPS'15, page 1135–1143, Cambridge, MA, USA. MIT Press.

Hassibi, B. and Stork, D. (1992). Second order derivatives for network pruning: Optimal brain surgeon. *Advances in neural information processing systems*, 5.

Hayou, S., Ton, J.-F., Doucet, A., and Teh, Y. W. (2021). Robust pruning at initialization. In *International Conference on Learning Representations*.

He, Y., Dong, X., Kang, G., Fu, Y., Yan, C., and Yang, Y. (2019). Asymptotic soft filter pruning for deep convolutional neural networks. *IEEE transactions on cybernetics*, 50(8):3594–3604.

He, Y., Zhang, X., and Sun, J. (2017). Channel pruning for accelerating very deep neural networks. In *2017 IEEE International Conference on Computer Vision (ICCV)*, pages 1398–1406.

Hoefler, T., Alistarh, D., Ben-Nun, T., Dryden, N., and Peste, A. (2021). Sparsity in deep learning: Pruning and growth for efficient inference and training in neural networks. *J. Mach. Learn. Res.*, 22(241):1–124.

Jordão, A. and Pedrini, H. (2021). On the effect of pruning on adversarial robustness. In *Proceedings of the IEEE/CVF International Conference on Computer Vision (ICCV) Workshops*, pages 1–11.

KIA Project Booklet (2022). KI Absicherung Overview and Poster Abstracts. https://www.ki-absicherung-projekt.de/fileadmin/KI_Absicherung/Final_Event/KI-A_poster-booklet_Onlineversion.pdf.

Kwon, S. J., Lee, D., Kim, B., Kapoor, P., Park, B., and Wei, G.-Y. (2020). Structured compression by weight encryption for unstructured pruning and quantization. In *Proceedings of the IEEE/CVF Conference on Computer Vision and Pattern Recognition*, pages 1909–1918.

LeCun, Y., Denker, J., and Solla, S. (1989). Optimal brain damage. *Advances in neural information processing systems*, 2.

Lee, N., Ajanthan, T., and Torr, P. H. (2018). Snip: Single-shot network pruning based on connection sensitivity. *arXiv preprint arXiv:1810.02340*.

Li, H., Kadav, A., Durdanovic, I., Samet, H., and Graf, H. P. (2016). Pruning filters for efficient convnets. *arXiv preprint arXiv:1608.08710*.

Li, Z., Chen, T., Li, L., Li, B., and Wang, Z. (2022). Can pruning improve certified robustness of neural networks? *arXiv preprint arXiv:2206.07311*.

Lin, M., Ji, R., Wang, Y., Zhang, Y., Zhang, B., Tian, Y., and Shao, L. (2020). Hrank: Filter pruning using high-rank feature map. In *Proceedings of the IEEE/CVF conference on computer vision and pattern recognition*, pages 1529–1538.

Liu, W., Anguelov, D., Erhan, D., Szegedy, C., Reed, S., Fu, C.-Y., and Berg, A. C. (2016). Ssd: Single shot multibox detector. In *European conference on computer vision*, pages 21–37. Springer.

Montavon, G., Lapuschkin, S., Binder, A., Samek, W., and Müller, K.-R. (2017a). Explaining nonlinear classification decisions with deep taylor decomposition. *Pattern Recognition*, 65:211 – 222.

Montavon, G., Lapuschkin, S., Binder, A., Samek, W., and Müller, K.-R. (2017b). Explaining nonlinear classification decisions with deep taylor decomposition. *Pattern recognition*, 65:211–222.

Nadizar, G., Medvet, E., Pellegrino, F. A., Zullich, M., and Nichele, S. (2021). On the effects of pruning on evolved neural controllers for soft robots. In *Proceedings of the Genetic and Evolutionary Computation Conference Companion*, pages 1744–1752.

Otter, D. W., Medina, J. R., and Kalita, J. K. (2020). A survey of the usages of deep learning for natural language processing. *IEEE transactions on neural networks and learning systems*, 32(2):604–624.

Samek, W., Montavon, G., Lapuschkin, S., Anders, C. J., and Müller, K.-R. (2021). Explaining deep neural networks and beyond: A review of methods and applications. *Proceedings of the IEEE*, 109(3):247–278.

Sehwag, V., Wang, S., Mittal, P., and Jana, S. (2020). Hydra: Pruning adversarially robust neural networks. In Larochelle, H., Ranzato, M., Hadsell, R., Balcan, M., and Lin, H., editors, *Advances in Neural Information Processing Systems*, volume 33, pages 19655–19666. Curran Associates, Inc.

Simonyan, K. and Zisserman, A. (2014). Very deep convolutional networks for large-scale image recognition. *arXiv preprint arXiv:1409.1556*.

Wang, X., Yu, F., Dou, Z.-Y., and Gonzalez, J. E. (2017). Skipnet: Learning dynamic routing in convolutional networks. *CoRR*, abs/1711.09485.

Weichert, D., Link, P., Stoll, A., Rüping, S., Ihlenfeldt, S., and Wrobel, S. (2019). A review of machine learning for the optimization of production processes. *The International Journal of Advanced Manufacturing Technology*, 104(5):1889–1902.

Ye, S., Xu, K., Liu, S., Cheng, H., Lambrechts, J., Zhang, H., Zhou, A., Ma, K., Wang, Y., and Lin, X. (2019). Adversarial robustness vs. model compression, or both? In *2019 IEEE/CVF International Conference on Computer Vision (ICCV)*, pages 111–120, Los Alamitos, CA, USA. IEEE Computer Society.

Zeng, W. and Urtasun, R. (2019). Mlprune: Multi-layer pruning for automated neural network compression.